Journal of Engineering Science 10(2), 2019, 69-78

JES
an international Journal

STRUCTURAL ANALYSIS OF A THICK-WALLED PRESSURE VESSEL USING FEM

Pial Das and Md. Shahidul Islam

Department of Mechanical Engineering, Khulna University of Engineering & Technology, Khulna, Bangladesh

Received: 30 April 2019 Accepted: 30 October 2019

ABSTRACT

The structural analysis of thick-walled pressure vessel is very important to maintain the reliability of the material. For analyzing various displacement and principal stress components. FEM (Finite Element Method) is very useful and practically applicable tool especially for structure with geometric discontinuity. Pressure vessel always contains some geometric discontinuity in many sorts of way. Such discontinuity is due to opening of the vessel causes stress concentration around it. This may lead to structural failure. The present analysis is done using ABAQUS 6.14 software within elastic limit. The main focus of this analysis is to compare the distribution of displacement and stress components for continuous, discontinuous structure and bimetallic (two heterogeneous metal) bonded joint for nozzle and find out the effect of hole in geometry of thick-walled pressure vessel. For getting more accurate result, eight nodes C3D8R cube and four nodes C3D10 tetrahedral type element is used for continuous and discontinuous model respectively. The result shows that the effect of pressure rise and geometric discontinuity is more significant for the Von-mises and Hoop stress.

Keywords: pressure vessel; stress concentration; size discontinuity; bi-metallic joint; FEM

1. INTRODUCTION

The main purpose of the thick-walled pressure vessel is to withstand very high pressure at different environment. Raju *et al.* (2015) showed that the pressure acting on pressure vessel may be constant or cyclic. In this present work constant pressure has been used for analysis. The opening of the pressure vessel leads to the high stress concentration which results in unexpected failure as ductile fracture of the vessel. Chelan *et al*. (2014) revealed that the geometric discontinuity affects the stress distribution in the pressure vessel structure and the elementary stress equations are no longer prevail. Multi-axial stress situation is governed in such pressure vessel which has been applied in this analysis. Clemens (2005) showed that for the safety concern, the pressure should be in the elastic limit and optimum safety factor must be used in the vessel design. So, in this analysis pressure within elastic limit has been used with proper safety factor. A lot of researchers have been interested in the field of pressure vessel. Josip and Nedelijko (2011) compared experimental solution obtained by strain gauge with the solution obtain by the finite element method. They concluded that maximum acceptable deviation limit is up-to 15.5% for von-miscs stress. Pravin and Kachare (2012) discussed about the optimum location of the opening for the vessel, which has been applied in this analysis. James *et al*. (2000) studied about the angle of the opening. Drazan and Ivan (2007) worked with thick walled pressure vessel with changeable head geometry. Drazan and Ivan (2007) also studied about the overloading effect of pressure vessel specially used for underground storage. No overloading has been used in this analysis. The pressure vessel with discontinuous and bi-metallic bonded joint structure is not clear until now. Therefore, the thick-walled pressure vessel with continuous, discontinuous and bi-metallic bonded joint structure is analyzed numerically in the present study. In this study, apart from main focus, the effect of internal pressure rise is investigated for different types of model. The effect of same thickness but increased radial size is also discussed in terms of displacements and stresses. The effect of stress concentration at the opening hole in the vessel is analyzed in term of Von-mises and Hoop stress.

2. GOVERNING EQUATIONS

The well-known elastic stress solution for thick walled pressure vessel was first developed by Lame. It gives solution for smooth and continuous cylinder.

$$\sigma_r = \left(\frac{p_a R_1^{\ 2} - p_b R_2^{\ 2}}{R_2^{\ 2} - R_1^{\ 2}} \right) - \frac{R_1^{\ 2} R_2^{\ 2}}{r^2} \frac{(p_a - p_b)}{R_2^{\ 2} - R_1^{\ 2}} \tag{1}$$

$$\sigma_\theta = \left(\frac{p_a a^2 - p_b b^2}{R_2^{\ 2} - R_1^{\ 2}} \right) + \frac{R_1^{\ 2} R_2^{\ 2}}{r^2} \frac{(p_a - p_b)}{R_2^{\ 2} - R_1^{\ 2}} \tag{2}$$

* Corresponding Author: shahidulbitk@gmail.com
https://www2.kuet.ac.bd/JES/

ISSN 2075-4914 (print); ISSN 2706-6835 (online)

$$\sigma_z = \left(\frac{p_a R_1^2 - p_b R_2^2}{R_2^2 - R_1^2} \right) \tag{3}$$

Whereσ_i, p_a, p_b, R_1, R_2, r represents normal stress, internal pressure, outside pressure, inner radius, outer radius, Distance from center of cylinder. For isotropic material, the property is constant in all direction. The stress for the three dimensional isotropic material is determined by Daryl (2009) as follows.

$$\begin{Bmatrix} \sigma_{rr} \\ \sigma_{\theta\theta} \\ \sigma_{\phi\phi} \\ \sigma_{r\theta} \\ \sigma_{\theta\phi} \\ \sigma_{\phi r} \end{Bmatrix} = \frac{E}{(1+\nu)(1-2\nu)} \begin{bmatrix} 1-\nu & \nu & \nu & 0 & 0 & 0 \\ \nu & 1-\nu & \nu & 0 & 0 & 0 \\ \nu & \nu & 1-\nu & 0 & 0 & 0 \\ 0 & 0 & 0 & \frac{1-2\nu}{2} & 0 & 0 \\ 0 & 0 & 0 & 0 & \frac{1-2\nu}{2} & 0 \\ 0 & 0 & 0 & 0 & 0 & \frac{1-2\nu}{2} \end{bmatrix} \begin{Bmatrix} \varepsilon_{rr} \\ \varepsilon_{\theta\theta} \\ \varepsilon_{\phi\phi} \\ \varepsilon_{r\theta} \\ \varepsilon_{\theta\phi} \\ \varepsilon_{\phi r} \end{Bmatrix} \tag{4}$$

Where σ_{ij}, ε_{ij}, E and ν represents the stress, strain, elastic constant and Poisson ration respectively.

2.1 Nomenclature

x, y, z	Cartesian co-ordinate	G	Shear modulus, MPa
$r\ \theta\ z$	Cylindrical co-coordinate	u_r	Deformation in radial direction
$\sigma_{xx}, \sigma_{yy}, \sigma_{zz}$	Normal stress in Cartesian co-ordinate, MPa	u_θ	Deformation in theta direction
$\sigma_{xy}, \sigma_{yz}, \sigma_{zx}$	Shear stress in Cartesian co-ordinate, MPa	u_z	Deformation in z direction
$\sigma_{xy}, \sigma_{yz}, \sigma_{zx}$	Normal stress in Cylindrical co-ordinate, MPa	ν	Poisson ratio
$\sigma_{r\theta}\ \sigma_{rz}\ \sigma_{\theta z}$	Shear stress in Cylindrical co-ordinate, MPa	r	Distance from origin, mm
$\varepsilon_{xx}, \varepsilon_{yy}, \varepsilon_{zz}$	Normal strain in Cartesian co-ordinate, MPa	R_1	Inner radius of cylinder
$\varepsilon_{xy}, \varepsilon_{yz}, \varepsilon_{zx}$	Shear strain in Cartesian co-ordinate, MPa	R_2	Outer radius of cylinder
$\varepsilon_{rr}, \varepsilon_{\theta\theta}, \varepsilon_{zz}$	Normal strain in Cartesian co-ordinate, MPa	p_a	Pressure on inner surface
$\varepsilon_{r\theta}, \varepsilon_{rz}, \varepsilon_{\theta z}$	Shear strain in Cylindrical co-ordinate, MPa	p_b	Pressure on outer surface
E	Young modulus, MPa	θ	Angle, degree

3. MODEL OF ANALYSIS

In this present analysis total eight models are used. Each one of them is a quarter part of full vessel to reduce computational time. They are recognized in two types, continuous model and model with discontinuity in structure. The hole is introduced in the geometry to create geometric irregularity. It is done to investigate the stress concentration around the hole.

Table 1: Models for analysis

Geometry	Model No	Inner radius R_1, mm	Outer radius R_2, mm	Wall Thickness t, mm	R_1/t	Hole Radius mm
Without hole (continuous)	1	45	60	15	3	---
	2	75	90	15	5	---
	3	120	135	15	8	---
	4	150	165	15	10	---
With hole (discontinuous)	5	45	60	15	3	10
	6	75	90	15	5	10
	7	120	135	15	8	10
	8	150	165	15	10	10

The paths along length *z* and thickness *t* for which data is taken are shown above. Where all continuous models are 15 mm in thickness and 150 mm in length along indicated path. And all discontinuous models are 15 mm in thickness and 140 mm in length along indicated path by red line. The mechanical properties of the material are shown in the following table. In the above Figure 1, (a) is simply a quarter of (c). Where in (c) p_a, p_b are internal pressure and outside pressure. In the current analysis the research questions are how the internal pressure rise with outside pressure set to zero, behaves with continuous and dis-continuous model.

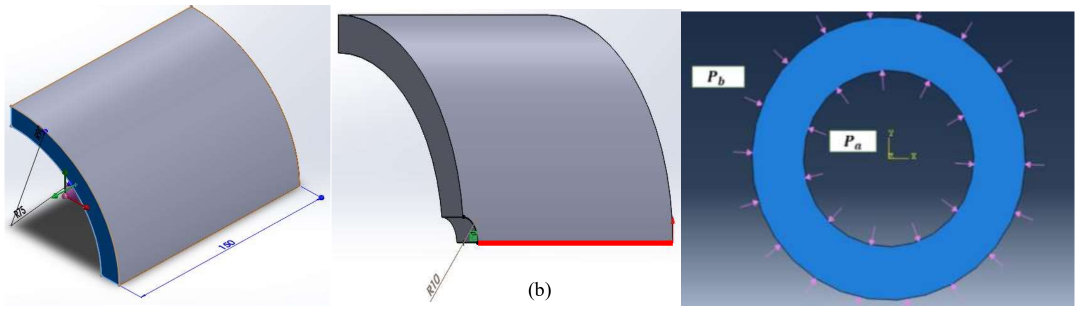

(a) (b) (c)

Figure 1: Models of cylinders

34CrMo4 alloy steel has been used as vessel material in this study. It is an isotropic material. This material is being increasingly used in the design and fabrication of the thick-walled pressure vessel. For bi-metallic nozzle joint, only nozzle material is taken of high carbon steel. Properties of both materials are taken from a published paper by Joseph *et al.* (2016).

Table 2: Mechanical properties of the material

Material	Modulus of elasticity E (MPa)	Poison ratio *v*	Tensile strength MPa	Yield strength MPa
34CrMo4 alloy steel	206×10^3	0.3	837	743
High carbon steel (S1100QL)	210×10^3	0.3	1145	1260

3.1 Boundary Conditions

In Figure 2 symmetry boundary conditions are used on the planes which are indicated by “s”. Internal pressure of the vessel is used of 38 MPa. It has been calculated by equation (2) for the model no 2. Tensile strength of 837 MPa is used as σ_θ with factor of safety 4. For simulating the boundary condition for a closed vessel end effect pressure force of 86.3636MPa which is calculated by equation (3) has been applied on the rear end surface of the model. The pressure on the outer surface was taken zero for both calculations. For other models the inner and outer surface pressure was taken 38MPa and zero as well, but different end effect pressure was applied which was calculated as before. For analyzing the effect of internal pressure on cylindrical vessel different safety factor of 3 and 2 was also used and the end effect pressure was also calculated for different internal pressure respectively. The end pressure effect for different safety factor is shown below.

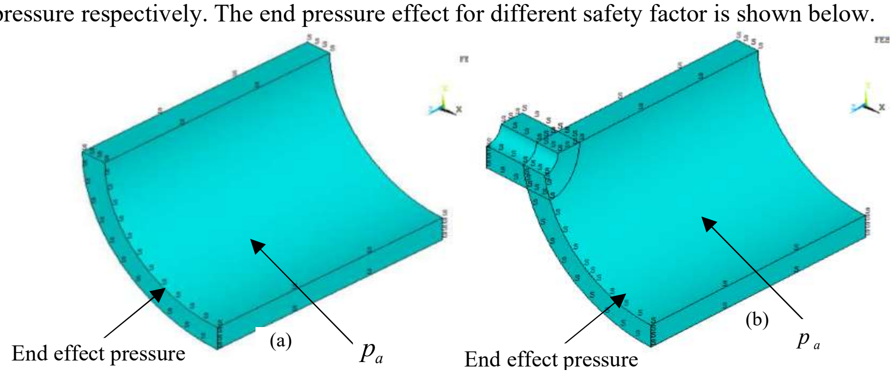

Figure 2: Boundary conditions of (a) model 2 (b) model 6

4. VERIFICATION OF PRESENT ANALYSIS

In this current work the result is compared with a published paper by Joseph *et al.* (2016). Verification is done for model 2 safety factor 4. By comparing the data from published paper and current work, the accuracy of the current work is determined. For the normal stress $\sigma_{\theta\theta}$ against thickness t for model 2, deviation is seen less than 1%, which is acceptable. Comparison of two results is shown in Figure 3.

Table 3: End pressure effect for different safety factor

Safety Factor	Model No	Internal pressure, MPa	Outside pressure, MPa	End effect pressure, MPa
	1	38	0	48.8571
	2	38	0	86.3636
	3	38	0	143.0588
4	4	38	0	180.9523
	5	38	0	48.8571
	6	38	0	86.3636
	7	38	0	143.0588
	8	38	0	180.9523
3	2	50.3114	0	114.3442
	6	50.3114	0	114.3442
2	2	75.4672	0	171.5163
	6	75.4672	0	171.5163

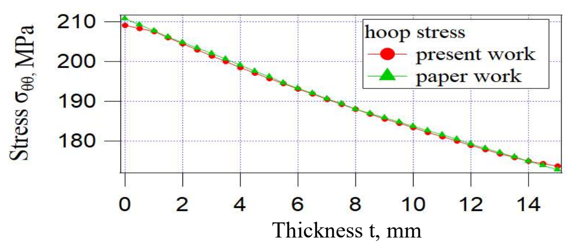

Figure 3: Verification of present analysis by paper work of Joseph *et al*. (2016).

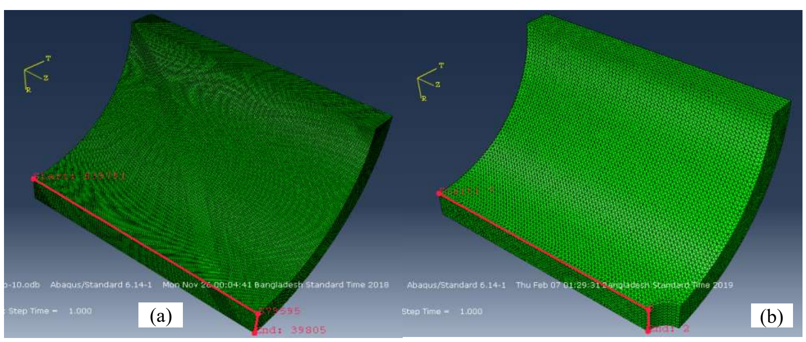

Figure 4: Meshed picture of the (a) model 2 (b) model 6

5. MESH DEPENDENCY TEST

The mesh dependency is checked by comparing the result from clement number 0.3 million to 4.6 million for model 2 with safety factor 4 and thickness of 15 mm. The result is shown in Figure 5. It is observed from the figure that the result remains constant from 0.8 million element number and farther. So, 0.8 million mesh elements are taken as optimum mesh number. This analysis is also done for other models as well.

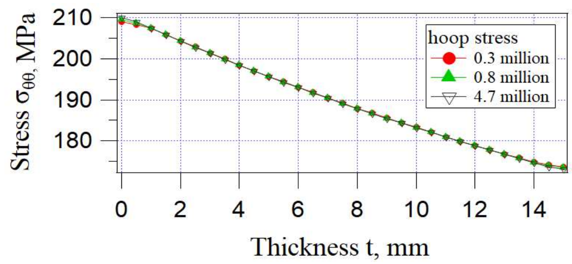

Figure 5: Mesh dependency check

6. RESULTS AND DISCUSSION

6.1 Maps of Displacement on r-z Plane of Model 2 and Model 6, Safety Factor 4

Here from figure 6 the surface plot (a) it can be seen that u_r does not vary along z for a given thickness. It only changes along t which is linear. Here for discontinuous model (b) the distribution is no longer linear. At $t = 0$ mm the u_r is more like sinusoidal curve along z. But at $t = 15$ mm where the effect of discontinuity is more significant their irregularities happen as the stress rises pretty quickly.

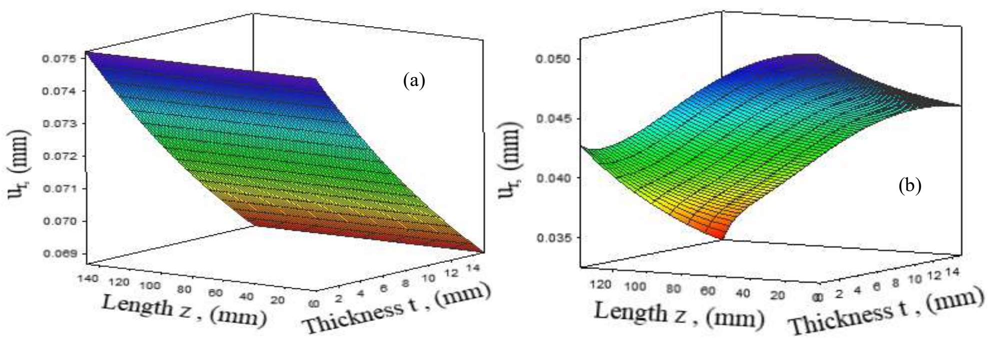

Figure 6: Distribution of displacement component. u_r (a) for model 2 (b) for model 6

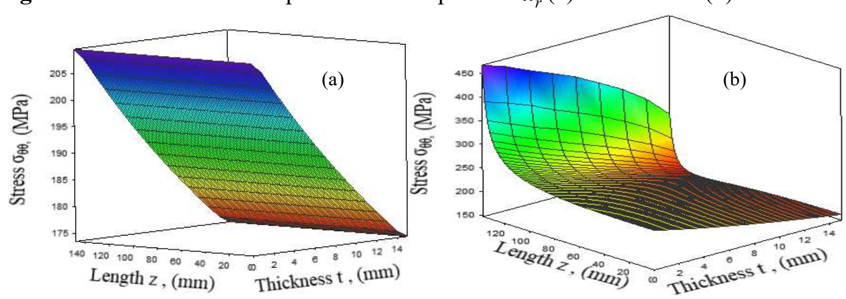

Figure 7: Distribution of $\sigma_{\theta\theta}$, (a) for model 2 (b) for model 6 with safety factor 4

6.2 Maps of Hoop Stress on r-z Plane for Model 2 and Model 6 with Safety Factor 4

Here from the Figure 7 it can be seen that for continuous model (a) hoop stress does not vary along z for a given thickness. It only changes along t which is linear. But for discontinuous model (b), it can be seen the stress concentration is lot more drastic at $t = 15$ mm as the curve suddenly rises where effect of discontinuity is more significant.

6.3 Distribution of Stress and Displacement for Model 2 at Constant Pressure

From the Figure 8 it can be observed that the displacement in the radial direction u_r is maximum in the inner surface and minimum at the outer surface. The change of displacement component in the z and θ direction is negligible and is almost zero. As the figure illustrated above it is observed that the stress σ_{rr} (normal stress in r face and r direction) is almost 38 MPa at the inner surface and almost 0 at the outer surface. $\sigma_{\theta\theta}$ which is the hoop stress is maximum at the inner surface and minimum at the outer surface. The stress σ_{zz} is constant along the thickness. On the other hand the share stress $\sigma_{r\theta}, \sigma_{rz}, \sigma_{\theta z}$ is almost zero along the thickness.

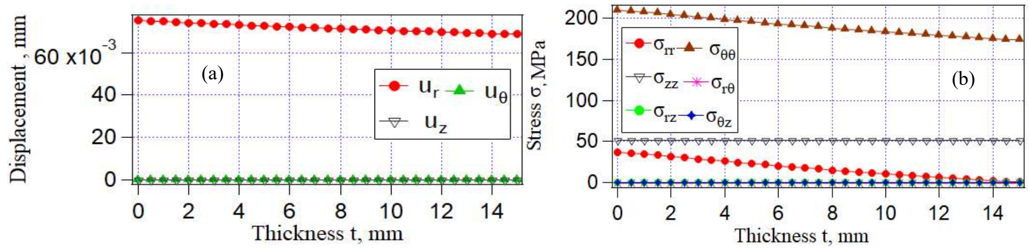

Figure 8: Distribution of varius (a) displacement and (b) stress components

6.4 Effect of Pressure Variation with Different Safety Factor for Model 2

As it can be seen from Figure 9 the higher pressure results in higher Von-mises stress. Another noticeable thing is in (a) the difference in the stresses caused by different internal pressure is higher in the inner surface than the outer surface i.e. the difference between the stress in the inner surfaces at $t = 0$ mm, between 50.3114 MPa and 75.4671 MPa is higher than same condition at $t = 15$ mm. It indicates that the effect of internal pressure rise is more significant in the inner surface in terms of Von-mises. Same fact also goes for $\sigma_{\theta\theta}$ in figure (b). The effect of internal pressure rise is only effective in the inner surface in terms of σ_{rr} stress as seen in Figure (c). In the outer surface σ_{rr} is zero for all magnitude of internal pressure.

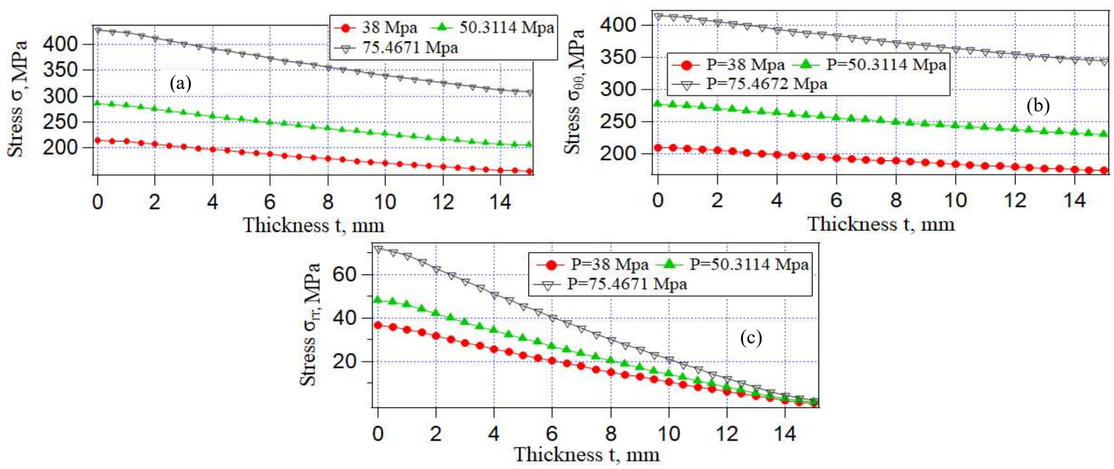

Figure 9: Distribution of (a) von-mises stress (b) $\sigma_{\theta\theta}$ (c) σ_{rr}

6.5 Effect of Size Variation for Continuous Models safety factor 4

It is seen from the figure 10illustrated above that the stress varies for the same applied pressure with different size of models. As R_1/t increase with different models, so do the stresses. The graphs represent that at inner surface ($t = 0$ mm) the difference among curves for von-mises stress (a) is same as for outer surface ($t = 15$ mm). Same phenomena occur for hoop stress (b). It indicates that the significance of the increased R_1/t is equal in both surfaces.

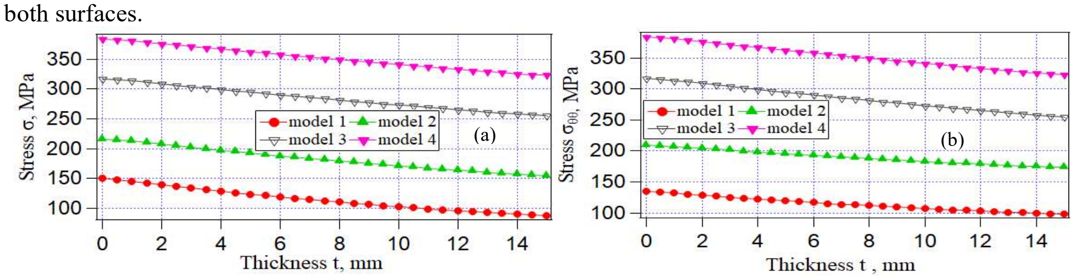

Figure 10: Distribution of (a) von-mises stress (b) hoop stress

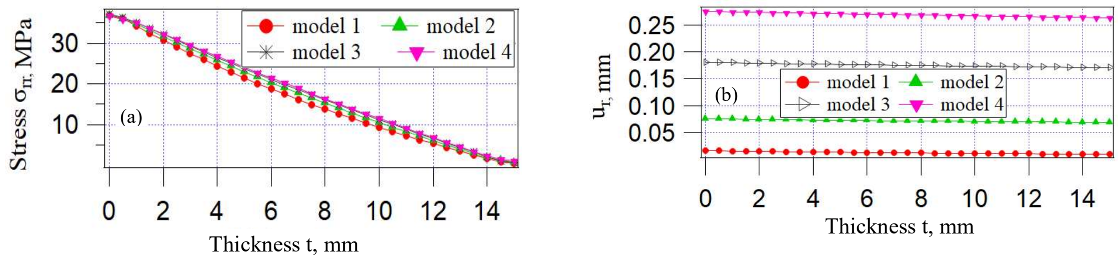

Figure 11: Distribution of (a) σ_{rr} and (b) u_r

From the Figure 11 it is seen that the effect of increased size has very little effect on σ_{rr}. For the higher values of R_1/t, the values of σ_{rr} is more consistent and varies linearly. Effect of R_1/t rise is equally significant in inner and outer surface in terms of u_r i.e. the difference between the curve of model 4 and model 5 at $t = 0$ mm is same as the difference at $t = 15$ mm.

6.6 Effect of Discontinuity for Safety Factor 4

It is clear from the figure 10 that von-mises stress (a) and hoop stress (b) increases incredibly when a hole as discontinuity is used in the geometry. It is also seen that the effect of discontinuity is more significant in the inner surface than outer one. Stress increases as three times in the inner surface where in the outer surface it increases as two times almost. Non-linearity in stress distribution is also seen for the models with hole toward the outer surface. Displacement magnitude (c) varies almost linearly for the discontinuous model also. Another interesting thing is displacement magnitude along the radius is smaller in values for the discontinuous model than the continuous one. It is because the element tends to bend near the opening. So, the radial displacement component decreases. That means displacement along the thickness of opening reduces significantly. Although the maximum displacement magnitude occurs in the inner surfaces.

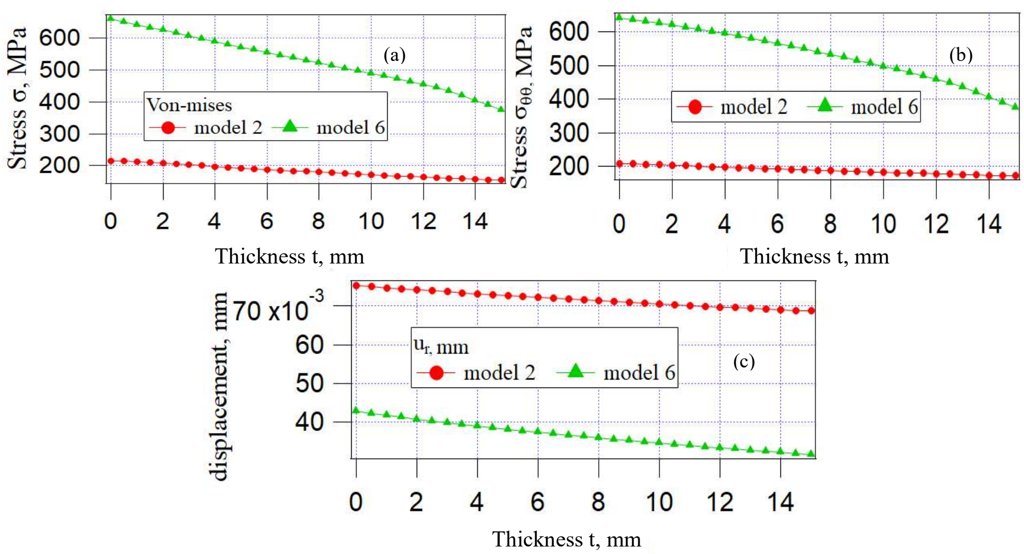

Figure 10: Distribution of (a) von–mises stress (b) hoop stress (c) u_r among continuous and discontinuous model.

6.7 Distribution of Stress for Different Discontinuous Model, Safety Factor 4

As illustrated in the figure 11 for every values of R_1/t the values of σ_{rr} remains almost same in the inner and outer surface. But the distribution is quite different. The stress starts from the negative values of almost 38 MPa and reaches to the highest value at almost the mid-point of the thickness of the hole and reduces to zero at the outer surfaces. It starts from negative value because the internal surface must oppose positive internal pressure of the cylinder. And it reaches to positive value because of the generation of internal residual energy due to geometric discontinuity. It indicates that normal stress in r direction and r face changes from compressive to tensile and come to zero. Higher the values of R_1/t results in higher maximum values of σ_{rr}.

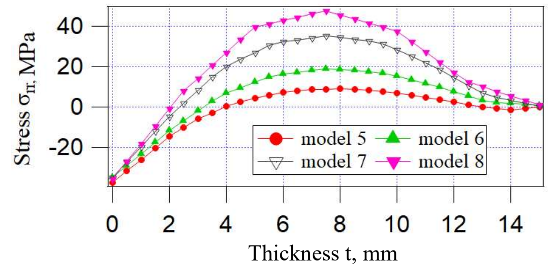

Figure 11: Effect of size variation on different discontinuous models

6.8 Distribution of Stress and Displacement for Continuous and Discontinuous Model with Different Pressure

As it can be seen the displacement component (a) varies almost linearly along the thickness for continuous model. Displacement magnitude reduces in the discontinuous model than continuous one at the same applied internal pressure. Here the effect of discontinuity on hoop stress (b) can be seen for different internal pressure for the same values of R_1/t. As it can be seen for the constant pressure the difference between stress of continuous and discontinuous model is higher for the higher pressure i.e. the difference between the stress in the inner surfaces for the model 2 and model 6 for the pressure of 50.3114 MPa is higher than same condition of 38 MPa. So, it can be seen the effect of pressure rise more significant in the higher pressure range. And this effect is more significant in the inner surface.

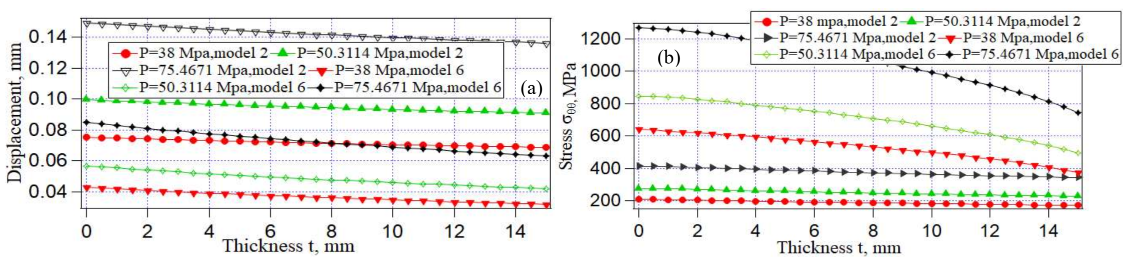

Figure 12: Distribution of (a) u_i (b) $\sigma_{\theta\theta}$ subjected to different internal pressure for model 2 and model 6.

6.9 Distribution of Stress and Displacement of Model 6 Safety Factor 4 along Length

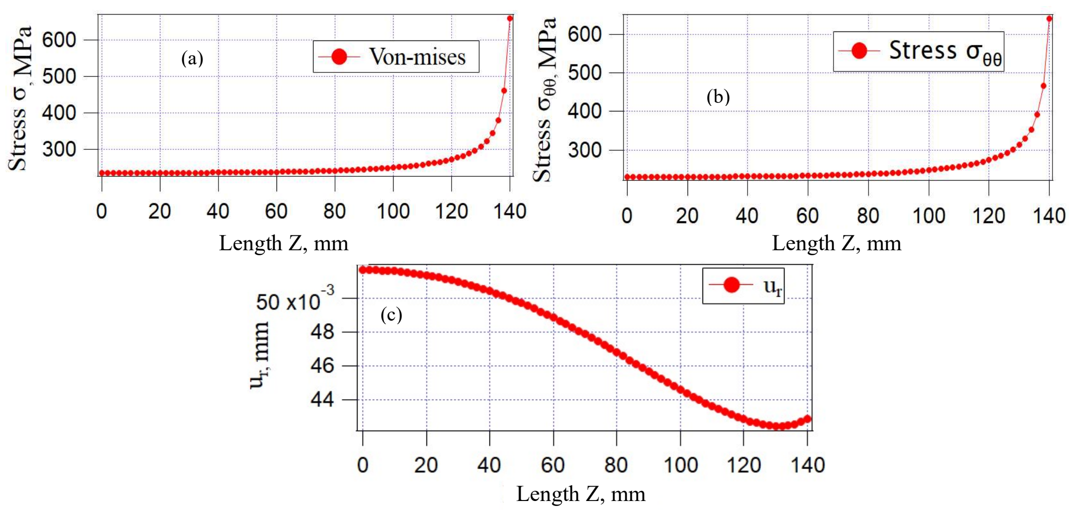

Figure 13: Distribution of (a) von-mises stress (b) hoop stress (c) u_r of model 6 along length

The effect of discontinuity (Figure 13) along the length is quite significant. The von-mises (a) and hoop (b) stresses are constant along the length for the continuous model. But the values of above both stresses starts to rise as points moves towards the opening hole for discontinuous model. At first the stress rises slowly but as the length reaches towards the hole the values of stress reach extremely high. The interesting thing is the rise of stress values is not gradual. At first the rate of increase is low but near the opening it is very high. Here it is clear from the Figure 13(c) that displacement component reduces along the length of the discontinuous model following a smooth curve. It falls at the lowest values near the hole and starts to rise right after because of the occurrence of the bending near the opening.

6.10 Bi-metallic Joint for Extended Nozzle

Here the cylinder and nozzle are made of 34CrMo4 and High carbon steel (S1100QL) ($E = 210$ GPa, $v = 0.3$) respectively. Mesh and geometry are merged between nozzle and model 6. Nozzle's inner and outer radius is 5 mm and 10 mm respectively and length is 20 mm.

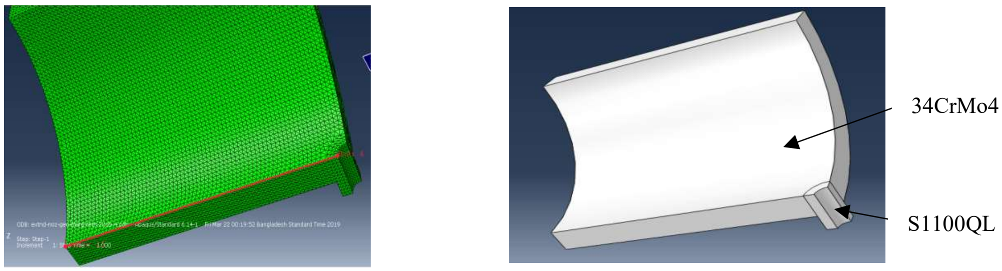

Figure 14: Model with external model

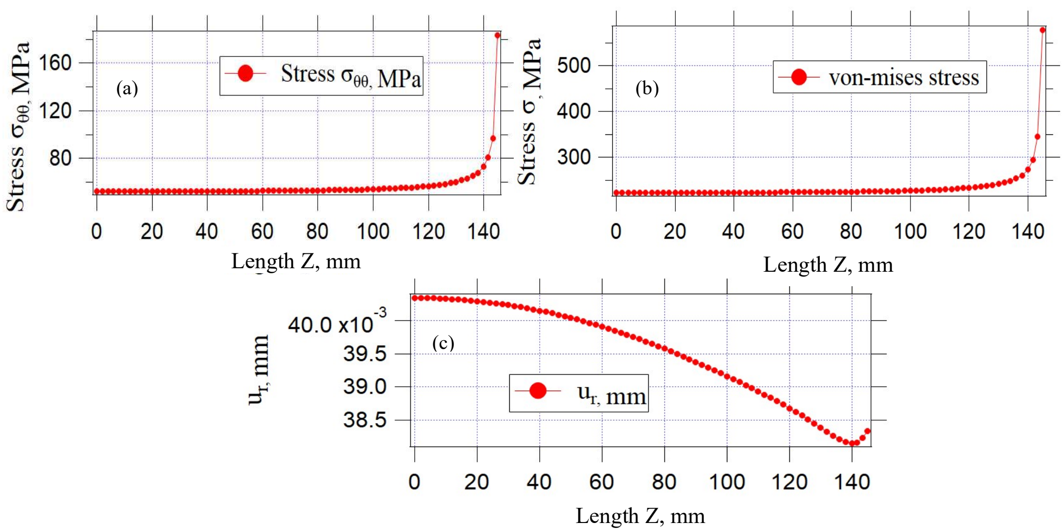

Figure 15: Distribution of (a) hoop stress (b) von-mises stress (c) u_r of extended nozzle model along length

As we can see from figure the effect of bi-metallic (two heterogeneous metal) joint is more rapidness in change of above stresses and displacement near the hole in comparison of model 6

7. CONCLUSIONS

In this work the displacement and different stress distribution for both continuous and discontinuous model subjected to internal pressure was analyzed. The effect of variation of internal pressure on both type of model is also discussed. Effect of discontinuity on different circular size of cylinder is analyzed. The numerical results lead to following conclusion.

- Displacement characteristic largely depends on the displacement in the radial direction.
- Effect of pressure rise, and geometric discontinuity is more significant for the Von-mises and Hoop stress.
- Effect of discontinuity on pressure rise is more significant in inner surface.
- Effect of size variation is equally significant on both inner and outer surface.
- Maximum stress concentration occurs around the irregularities of structure.

REFERENCES

Chelan P. Vora, and Shyam R. Gupta, 2014. A Review Paper on Pressure Vessel Design and Analysis, *Int. J. of Eng. Res. & Tech.*, 3. 40-45.

Daryl L. Logan, 2009. Appendix C, A First Course in the Finite Element Method, CENGAGE Learning, 4th Ed., 748-751.

Clemens Kaminski. 2005. Stress Analysis of Pressure Vessels, University of Cambridge.

Drazan Kozak, and Ivan Samardzic, 2007. Overloading Effect on the Carrying Capacity of Cylindrical Tank with Tori spherical Heads for the Underground Storage of Petrol, *Int. J. of Eng, Res. & Tech.,* 23.

Drazan Kozak, and Ivan Samardzic, 2007. Stress Analysis of Cylindrical Vessel with Changeable Head Geometry, *Science Bulletin, Sefic C.* 23.

James J. Ku, Benedict C. Sun, and Bernard Koplik, 2000. Local Pressure Stress on Lateral Pipe-Nozzle with Various Angles of Intersection, *Nuclear Engineering and Design*, 199, 335-340.

Joseph Mutava, Oncsmus Muvengei, Kenneth Njoroge, and John Kihiu, 2016. Finite Element Structural Analysis of a Thick-walled Pressure Vessel, *Proceedings of the 2016 Annual Conference on Sustainable Research and Innovation*, 174-185.

Joship Kacmarcik, and Nedelijko Vukojevic, 2011. Comparison of Design Method for Opening in Cylindrical Shells Under Internal Pressure Reinforced by Flush (Sct-On) Nozzles, *Int. J. of App. Mech. and Eng.*, 4.

Previa Mamie, and P.S. Kacharc, 2012. Structural Analysis of Nozzle Attachment on Pressure Vessel Design, *Int. J. of Eng. Res. & App,* 2. 1353-1358.

Raju, G., Hari K. Balm, Siva Nagaraju N., and Kirau K., 2015. Design and Analysis of Stress on Thick-walled Cylinder with and without Holes, *Int. J. of Eng. Res. & App.,* 5. 75-83.